Thermal effects in domain wall motion: Micromagnetic simulations and analytical model

E. Martinez*
Departamento de Ingenieria Electromecanica, Universidad de Burgos, Plaza Misael Banuelos s/n, E-09001 Burgos, Spain

L. Lopez-Diaz, L. Torres, and C. Tristan
Departamento de Fisica Aplicada. Universidad Salamanca, Plaza de la Merced s/n, E-37008 Salamanca, Spain

O. Alejos
Departamento Electricidad y Electronica, Universidad de Valladolid, Prado de la Magdalena, E-47071 Valladolid, Spain
(Received 13 November 2006; published 7 May 2007)

Micromagnetic simulations are used to study the effect of thermal fluctuations in domain wall motion driven by either an external field or an in-plane spin-polarized current in ferromagnetic nanowires of rectangular cross section. For wires with no edge roughness, simulations reveal that thermal effects do not significantly modify field-driven and current-driven domain wall dynamics at $T=0$ if nonadiabatic contributions are taken into account in the latter. If the perfect adiabatic approximation is assumed, however, no-null velocities are obtained for currents smaller than the critical value below which there is no domain wall propagation in the deterministic case. In order to mimic experimental conditions and carry out more realistic simulations, we have introduced some edge roughness in the nanowire, which leads into a characteristic pinning force for domain walls. If the driving force, either field or current, is large enough to overcome the roughness pinning force, the wall velocities are found to be similar to those at $T=0$. However, finite positive velocities are obtained for fields and currents smaller than the deterministic depinning threshold when thermal perturbations are included. In this thermally activated regime, the velocity increases exponentially with both field and current. Moreover, our results are found to be in good quantitative agreement with some experimental data. In the last part of this work, the one-dimensional model for domain wall motion derived by Li *et al.* [J. Appl. Phys. **99**, 08Q702 (2006)] is extended to include thermal perturbations following the Langevin formalism of the Brownian motion. The predictions of the model are compared with those of micromagnetic simulations finding good agreement between them.

DOI: 10.1103/PhysRevB.75.174409 PACS number(s): 75.75.+a, 75.40.Mg, 75.40.Gb, 75.10.Hk

I. INTRODUCTION

In recent years, domain wall motion (DWM) along thin ferromagnetic strips has become a source of much theoretical[1–28] and experimental[29–41] research. Its potential technological applications include magnetic random access memory[29] and logic devices.[30] Understanding and controlling the dynamics of a domain wall (DW) means, on a mesoscopic level, understanding and controlling magnetization reversal: except for thin samples of reduced lateral dimensions, in which the precessional switching dominates, domain wall propagation is the most effective way to revert magnetization.

The traditional way to move a DW is by applying a magnetic field H_{ext}. In Ref. 25, Thiaville *et al.* showed that, if the transverse dimensions of the strip are small enough, DW velocities obtained from micromagnetic simulations agree well with those predicted by Walker's one-dimensional analytical model.[1,2] A more realistic approach was carried out in Ref. 23 including roughness along the wire edges. The results were found to fit well with experimental data[33] in an intermediate viscous field range, where the velocity increases with field. For large fields, the simulations predict a saturating behavior up to the breakdown Walker field H_W, whereas experimental DW velocities are found to increase monotonically in the range analyzed. On the other hand, for small fields, the simulations predict a threshold value of the applied field H_{unp} below which the DW ends up pinned at some local defect, whereas a smooth transition toward the linear regime is found experimentally. In this work, we will extend this investigation including the effect of thermal fluctuations which, to our knowledge, has not been done so far. In particular, we will show how thermal fluctuations smooth out the abrupt transition from the pinned to the viscous regime, yielding a better agreement with the experimental data.

It is also possible to move a DW by means of an electrical current flowing through the wire. This phenomenon was theoretically predicted by Berger[4] and Slonczewski[5] and later on verified experimentally.[38–41] However, the final theory for describing the spin torque mechanism still remains as a challenging problem. Some authors have claimed that if the domain wall width is larger than a typical characteristic length, adiabatic conditions are fulfilled and, consequently, the spin of conduction electrons become fully polarized due to the local magnetization. The typical characteristic length to which the DW width has to be compared is, depending on the on the model, the spin-diffusion length,[7] the Larmor precession length,[8] or the Fermi wavelength.[9] If this perfect adiabatic approximation is assumed, the simulations predict a critical current j_{cri} below which DWM is not observed, which is more than ten times larger than those measured in the experiments.[38,40] For this reason, other authors have claimed that nonadiabatic corrections must be included for a finite wall width.[13,16,27] Taking into account a nonadiabatic term in the formalism leads to no-null velocities for the current-density values used in the experiments,[27] but the computed velocities are one or two orders of magnitude larger than those measured experimentally.[38,40] In this work,

we will show that thermal fluctuations have a significant impact on spin torque driven DWM and how taking them into account help us in reducing the gap between theory and experiments.

The paper is organized as follows. First, the basic features of our micromagnetic model are discussed along with the numerical details of the simulations (Sec. II). In Sec. III, DWM driven by an external field applied along the wire axis is studied for both perfect and rough wires, comparing the deterministic results ($T=0$ K) with the ones at finite temperature. Later on, current-driven DWM is discussed (Sec. IV). Both adiabatic and nonadiabatic approaches will be discussed for both perfect and rough wires. Finally, in Sec. V, we show that the micromagnetic results can be qualitatively explained from an analytical point of view using a simple one-dimensional model (1DM) that includes thermal effects. The main conclusions of our work are presented in Sec. VI.

II. MICROMAGNETIC MODEL AND NUMERICAL DETAILS

Our model is based on numerically solving the dynamic equation for the magnetization by discretizing the computational region by means of a finite-difference scheme. Thermal fluctuations are included by adding a random-fluctuating thermal field $\vec{H}_{th}$ to the effective field $\vec{H}_{eff}$ in Gilbert's dynamic equation[42,43]

$$\frac{d\vec{M}}{dt} = -\gamma_0 \vec{M} \times (\vec{H}_{eff} + \vec{H}_{th}) + \frac{\alpha}{M_s}\left(\vec{M} \times \frac{d\vec{M}}{dt}\right), \quad (1)$$

where γ_0 is the gyromagnetic ratio and α is the Gilbert damping constant. The thermal field $\vec{H}_{th}$ is assumed to be a Gaussian random process verifying the following statistical properties:[42,43]

$$\langle H_{th,i}(\vec{r},t)\rangle = 0, \quad (2)$$

$$\langle H_{th,i}(\vec{r},t) H_{th,j}(\vec{r}',t')\rangle = 2D_{\mu M}\delta_{ij}\delta(\vec{r}-\vec{r}')\delta(t-t'). \quad (3)$$

The strength of the thermal field, which follows from the fluctuation-dissipation theorem, is given by

$$D_{\mu M} = \frac{\alpha K_B T_{\mu M}}{\gamma_0 \mu_0 M_s \Delta x^3}, \quad (4)$$

where Δx is the cell size and K_B is the Boltzmann constant. $T_{\mu M}$ represents the effective micromagnetic temperature. Therefore, the thermal field can be expressed as

$$\vec{H}_{th}(\vec{r},t) = \vec{\eta}(\vec{r},t)\sqrt{\frac{2\alpha K_B T_{\mu M}}{\gamma_0 \mu_0 M_s \Delta x^3 \Delta t}}, \quad (5)$$

where Δt is the time step used to numerically integrate the Langevin equation, and $\vec{\eta}$ is an stochastic vector whose Cartesian components $i:x,y,z$ are Gaussian-distributed random numbers satisfying the following statistical properties:

$$\langle \eta_i(\vec{r},t)\rangle = 0, \quad (6)$$

$$\langle \eta_i(\vec{r},t)\,\eta_j(\vec{r}',t')\rangle = \delta_{ij}\delta(\vec{r}-\vec{r}')\delta(t-t'). \quad (7)$$

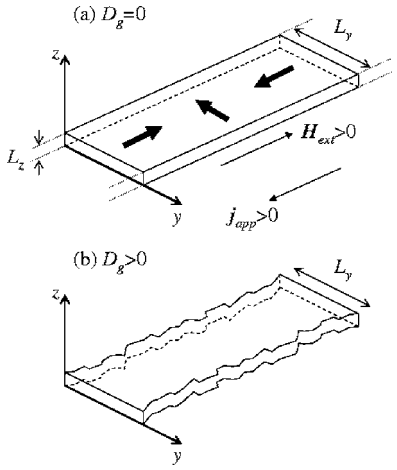

FIG. 1. Schematic representation of the simulated geometry. (a) Perfect wires. (b) Wires with edge roughness.

The effective field $\vec{H}_{eff}$ in Eq. (1) includes exchange, self-magnetostatic, and external field contributions. The first one is computed by means of the six-neighbor representation,[44] whereas the second one is evaluated assuming that the magnetization is uniform inside each computational cell.[45]

Equation (1) is the dynamic equation to be solved when the external field is the driving force.[46] For current-driven DWM, Eq. (1) must be modified to take into account for the spin-transfer torque contribution[16] as follows:

$$\frac{d\vec{M}}{dt} = -\gamma_0 \vec{M} \times (\vec{H}_{eff} + \vec{H}_{th}) + \frac{\alpha}{M_s}\left(\vec{M} \times \frac{d\vec{M}}{dt}\right) + b_J(\vec{u}_x \cdot \nabla)\vec{M} - \frac{c_J}{M_s}\vec{M} \times (\vec{u}_x \cdot \nabla)\vec{M}, \quad (8)$$

where the coefficients b_J and c_J are given by $b_J = \frac{(j_{app}\mu_B P)}{eM_s}$ and $c_J = \xi b_j$, with j_{app} being the electrical current density, μ_B the Bohr magneton, P the spin polarization of the current, and e the electron's electric charge. The coefficient ξ is a dimensionless constant describing the degree of nonadiabaticity between the spin of conduction electrons and the local magnetization.[16]

A schematic representation of the problem under study is displayed in Fig. 1. The computational region is a 2-μm-long portion of an infinite wire of transverse dimensions $L_y \times L_z$ with a head-to-head domain wall initially located in the middle separating two semi-infinite opposite domains. The infiniteness of the wire is simulated by removing the magnetic charges appearing at both ends of the computational region. Also, in order to minimize spurious effects that appear when the domain wall approaches the artificial end, a moving computational region is considered in such a way that the wall is always at the center. On the other hand, natural edge roughness is simulated following a similar procedure done in Ref. 23 by randomly removing regions from the wire edges with a uniform probability distribution characterized by the typical roughness size D_g. A 40-μm-long edge roughness pattern is generated at the beginning of the

simulation to be used by the moving 2-μm-long computational region.

In the results that will be presented in the forthcoming sections, the following values have been considered as the intrinsic parameters of the model, all of which are typical of permalloy: $M_s=8.6\times10^5$ A/m, $A=1.3\times10^{-11}$ J/m, $K=0$, $\alpha=0.02$, $P=0.4$, and $\xi=0.04$. In order to compare our results with the experiment,[33] the transversal dimensions used for studying field-driven DWM are $L_y\times L_z=200\times5$ nm^2, whereas for current-driven DWM, a cross section $L_y\times L_z=50\times5$ nm^2 is considered. The dynamic stochastic equations [Eqs. (1) and (8)] are solved numerically using a fourth-order Runge-Kutta scheme interpreted in the Stratonovich sense.[47] The time step is 0.5 ps, and it was verified in several test cases that a value of 0.2 ps did not change the presented results. On the other hand, most of the results presented here were obtained by using a two-dimensional spatial discretization mesh of cubic cells with $\Delta x=5$ nm, but it was confirmed that the results do not significantly change when the cell size was refined to half in a three-dimensional mesh for several tested cases.

III. FIELD-DRIVEN DOMAIN WALL MOTION

A. Perfect wires ($D_g=0$)

Starting from the initial state, which consists of a transverse head-to-head wall in equilibrium, an external field is instantaneously applied and the time evolution of the domain wall velocity is monitored. The results for different values of H_{ext} are collected in Fig. 2(c). As can be observed, the velocity increases with the field strength up to the so-called micromagnetic Walker field H_W. For smaller fields ($H_{ext}<H_W$), the wall, after a short transient period, reaches a constant velocity at $T=0$ K [Fig. 2(a)]. At $T=300$ K, however, the DW instantaneous velocity $v(t)$ does not reach a constant value but fluctuates due to the thermal noise [see Fig. 2(a)]. Nevertheless, the time-averaged value of $v(t)$ coincides with the constant velocity at $T=0$ K, as can be observed in Fig. 2(c). On the other hand, as depicted in Fig. 2(b), for $H_{ext}>H_W$, DWM is turbulent and the average velocity falls to a low value for both $T=0$ K and $T=300$ K. As it has already been discussed by Nakatani *et al.*,[23] in this regime, the DW velocity experiments accelerations and decelerations related to the nucleation and annihilation of an antivortex. From the results depicted in Fig. 2(c), we conclude that in the absence of surface roughness, the thermal fluctuations do not significantly affect the DWM.

B. Rough wires ($D_g\neq0$)

A similar analysis to the one presented in the previous section has been carried out for wires with different degrees of roughness. The results at $T=0$ K are given in Fig. 3(a). As can be observed, edge roughness greatly impacts DWM. On one hand, it leads to an increase in the breakdown field H_W, from 2.75 mT (perfect wire) up to 15 mT when $D_g=10$ nm (not shown). On the other hand, an unpinning threshold field [$H_{unp}(0\text{ K})$] appears below which there is no DW propagation because the wall is pinned by the roughness. This unpinning threshold is found to increase with roughness from $\mu_0H_{unp}(0\text{ K})\approx2$ mT for $D_g=10$ nm up to $\mu_0H_{unp}(0\text{ K})\approx4$ mT for $D_g=25$ nm. A similar analysis was already performed by Nakatani *et al.*[23] Moreover, they showed that by choosing $D_g=20$ nm, the computed velocities fit well the experimental observations of Ref. 33 for a small field range, called viscous regime, in which DW velocity increases almost linearly with H_{ext}. However, their simulations at $T=0$, in the same manner than ours [Fig. 3(a)], predict an abrupt jump from the pinned to the viscous regime at $H_{ext}=H_{unp}(0\text{ K})$, whereas a smooth transition is found experimentally.[33] Thermal activation over the pinning energy barriers could lead to no-null DW velocities for $H_{ext}<H_{unp}(0\text{ K})$ and, consequently, improve the agreement between the experiments and the simulations.

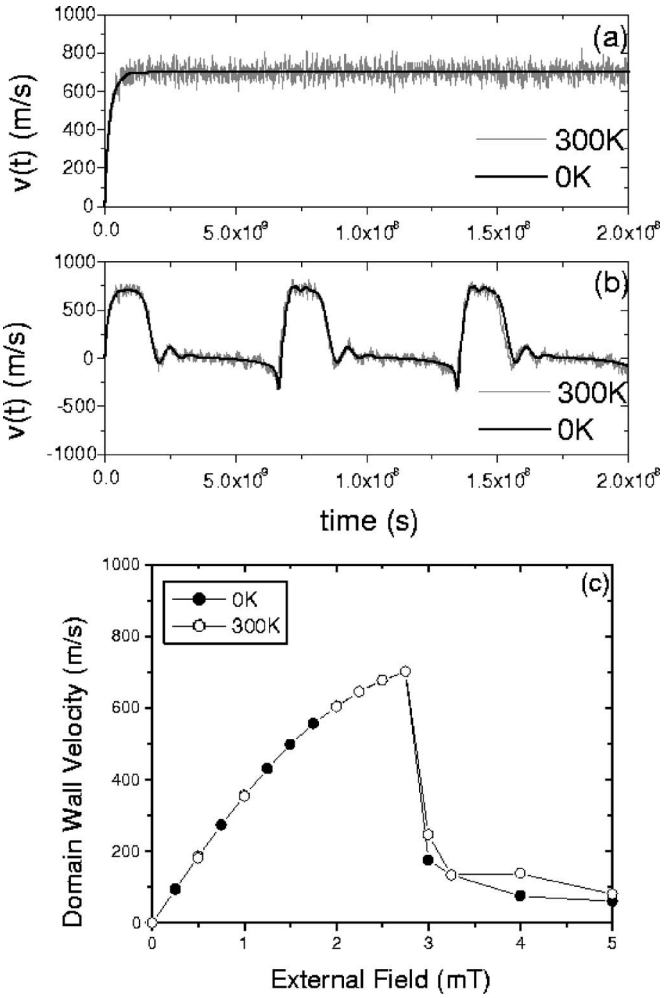

FIG. 2. Time evolution of the instantaneous DW velocity driven by an external field. (a) Below H_W, $\mu_0H_{ext}=2.75$ mT and (b) above H_W, $\mu_0H_{ext}=3.25$ mT in a nanowire of 200×5 nm^2 cross section. (c) Averaged DW velocity as a function of the applied field.

The same set of simulations described in the previous paragraph was carried out at $T=300$ K. The results are collected in Fig. 3(b). Each point in the graph has been obtained by averaging in time over the last 90 ns of the temporal window (100 ns) and also averaging over ten stochastic realizations. As can be observed, the unpinning field is slightly

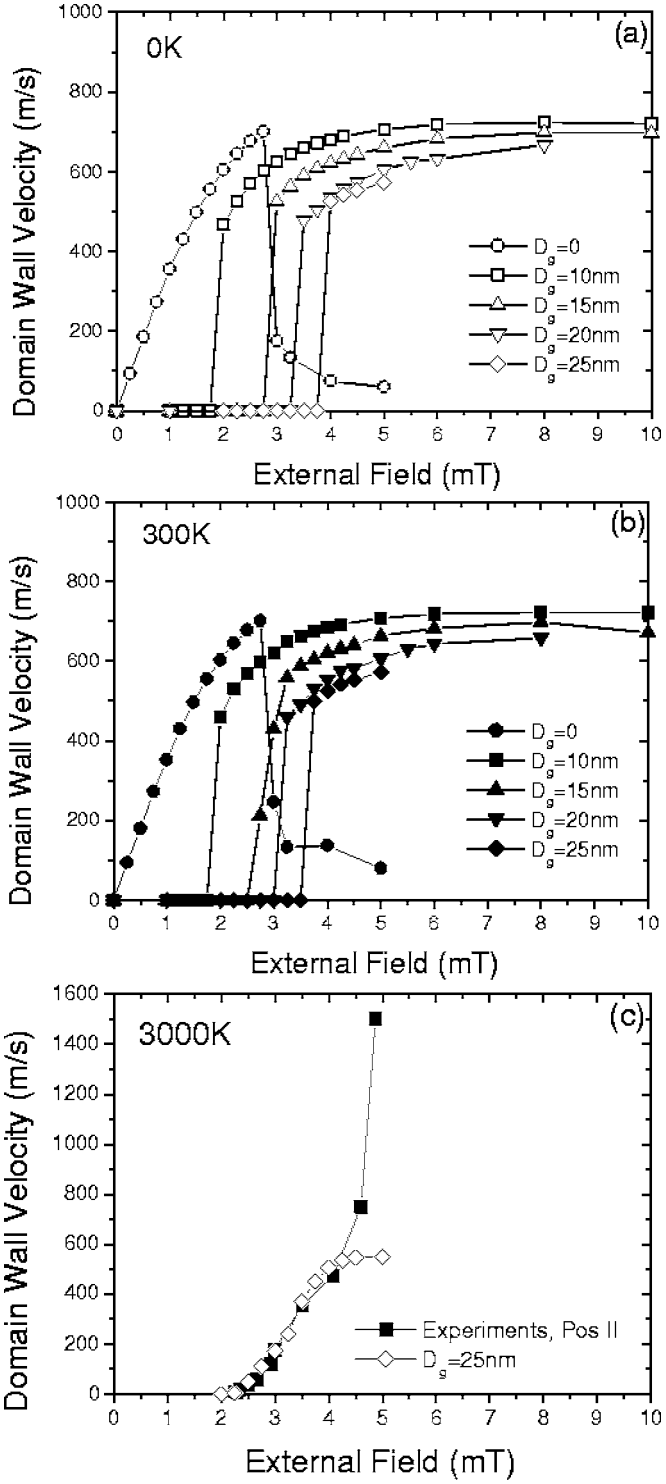

FIG. 3. Time-averaged DW velocity in a strip of 200×5 nm^2 cross section for different grain sizes at (a) $T_{\mu M}=0$ K, (b) $T_{\mu M}=300$ K, and (c) $T_{\mu M}=3000$ K. In (c), the experimental values (Ref. 33), measured at room temperature, are also shown.

reduced with respect to the deterministic case, but the transition from the pinned to the viscous regimes continues to be abrupt. Therefore, we are underestimating the effect of thermal perturbations in our Langevin simulations with respect to the experiments. There are at least two reasons for this. On

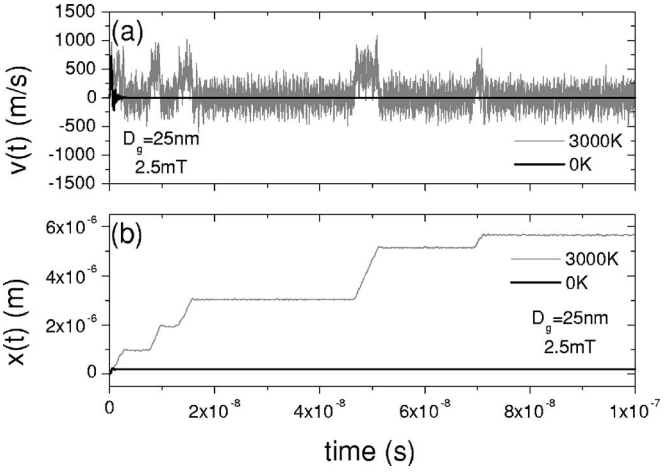

FIG. 4. Time evolution of DW velocity $v(t)$ and position $x(t)$ along a rough wire (200×5 nm^2, $D_g=25$ nm) driven by external field of $\mu_0 H_{ext}=2.5$ mT. Deterministic dynamics ($T_{\mu M}=0$ K) is compared with an individual stochastic trajectory at $T_{\mu M}=3000$ K.

one hand, the temporal window of the simulations (100 ns) is much smaller than that of the experiments[33] and, as it is well known, the probability of occurrence of thermally activated processes increases with time. On the other hand, by discretizing our computational region, we are not considering thermal perturbations occurring at length scales smaller than our cell size. This leads to some unphysical results, such as an overestimation of the Curie temperature by roughly 1 order of magnitude.[48] Although some attempts have been made to correct for this kind of inconsistencies,[49] the inclusion of thermal perturbations in micromagnetic simulations is still a challenging problem and some aspects of it are not well understood yet. Nevertheless, in view of what has been said before, it is clear that, for the problem that concerns us, the parameter $T_{\mu M}$ of our model must be significantly higher than the real temperature T if we want to estimate the effect of thermal perturbations correctly. Consequently, we repeated the simulations at higher values of $T_{\mu M}$ and found that the best agreement with the experimental data is obtained for $T_{\mu M}=3000$ K and $D_g=25$ nm. The comparison between the experimental data and the simulations is shown in Fig. 3(c). As can be observed, the thermally activated regime is reproduced accurately for fields up to $\mu_0 H_{ext}=4$ mT.[33] The comparison is made with the experimental measurements from position II since, as in our case, they correspond to the DW traveling along a straight section of the wire.[50] The fact that the value of $T_{\mu M}$ is larger than the real temperature by a factor of 10 should not be surprising since, as we mentioned before, the Curie temperature for our discretization is overestimated by roughly the same factor.[48]

In order to gain some understanding of thermally activated DWM, the time evolution of the DW position and velocity is shown in Fig. 4 for a typical stochastic trajectory at $T_{\mu M}=3000$ K and also for the deterministic case when the applied field is $\mu_0 H_{ext}=2.5$ mT and the roughness size $D_g=25$ nm. At $T=0$ K, the wall gets pinned after a few nanoseconds at a region of high local roughness and remains there for the rest of the time. On the contrary, at $T_{\mu M}=3000$ K, the wall also gets pinned, but after some

time, thermal fluctuations lead to the depinning of the DW. Once depinned, the wall moves at a steady velocity [notice the constant slope in the jumps of Fig. 4(b)] until it becomes pinned again. Therefore, the wall exhibits a jerky motion,[51] consisting of a sequence of random jumps. Although the time evolution of the DW position and velocity are not measured directly in Ref. 33, our results are consistent with their measurements of the probability of nonswitching (see Fig. 2 of Ref. 33).

IV. CURRENT INDUCED DOMAIN WALL MOTION

A. Perfect adiabatic limit ($\xi=0$)

1. Perfect wires ($D_g=0$)

In Fig. 5, the temporal evolution of the DW (a) velocity and (b) position are depicted for a current density $j_{app}=2.2\times10^{13}$ A/m^2 both at $T_{\mu M}=0$ K and $T_{\mu M}=3000$ K. In Fig. 5(c), the averaged velocities as a function of the current density are shown. As can be observed, at $T_{\mu M}=0$ K, there exists a threshold current $j_{cri}(0\text{ K})=2.4\times10^{13}$ A/m^2 [$b_{J,cri}(0\text{ K})=650$ m/s] below which no steady DW motion is observed. Above this value, the DW moves via nucleation and disappearance of antivortices, and the averaged DW velocity increases as $\mu_B P[j_{app}^2-j_{cri}^2(0\text{ K})]^{1/2}/[eM_s(1+\alpha^2)]$ as theoretically predicted.[9,26] On the other hand, at $T_{\mu M}=3000$ K, finite no-null DW velocities are obtained for applied currents smaller than the threshold $j_{cri}(0\text{ K})$. In this thermally activated regime, the averaged velocities increase exponentially with j_{app}. For larger currents, $j_{app}>j_{cri}(0\text{ K})$, the computed velocities are very similar to the ones obtained in the deterministic case. The time evolution of the instantaneous DW displacement [see Fig. 5(b)] presents an irregular staircase behavior related to the internal changes of the DW structure.

2. Rough wires ($D_g\neq0$)

The simulations of the previous section have been repeated for a wire with typical surface roughness $D_g=5$ nm. The results (not depicted here) are very similar to those of a perfect wire of the same dimensions [Fig. 5(c)]. Therefore, we conclude that, in the adiabatic approximation ($\xi=0$), the DW velocity is not hardly affected by the surface pinning arising from sample irregularities for typical permalloy grain sizes.[9] In any case, the computed minimum current density necessary to promote steady DWM ($\approx1.2\times10^{13}$ A/m^2) is far from the experimental measured values [$\approx(2-3)\times10^{12}$ A/m^2 in Ref. 38]. As it has already been pointed out,[27] the inclusion of nonadiabatic corrections is necessary in order to reproduce experimental results quantitatively.

B. Nonadiabatic approximation ($\xi>0$)

1. Perfect wires ($D_g=0$)

Temporal evolutions of both DW velocity and displacement are depicted in Fig. 6 for a perfect wire ($D_g=0$) in the nonadiabatic approximation with $\xi=0.04$ and the same parameters values used in Sec. IV A. The average velocities as a function of the applied current are plotted in Fig. 6(c). In

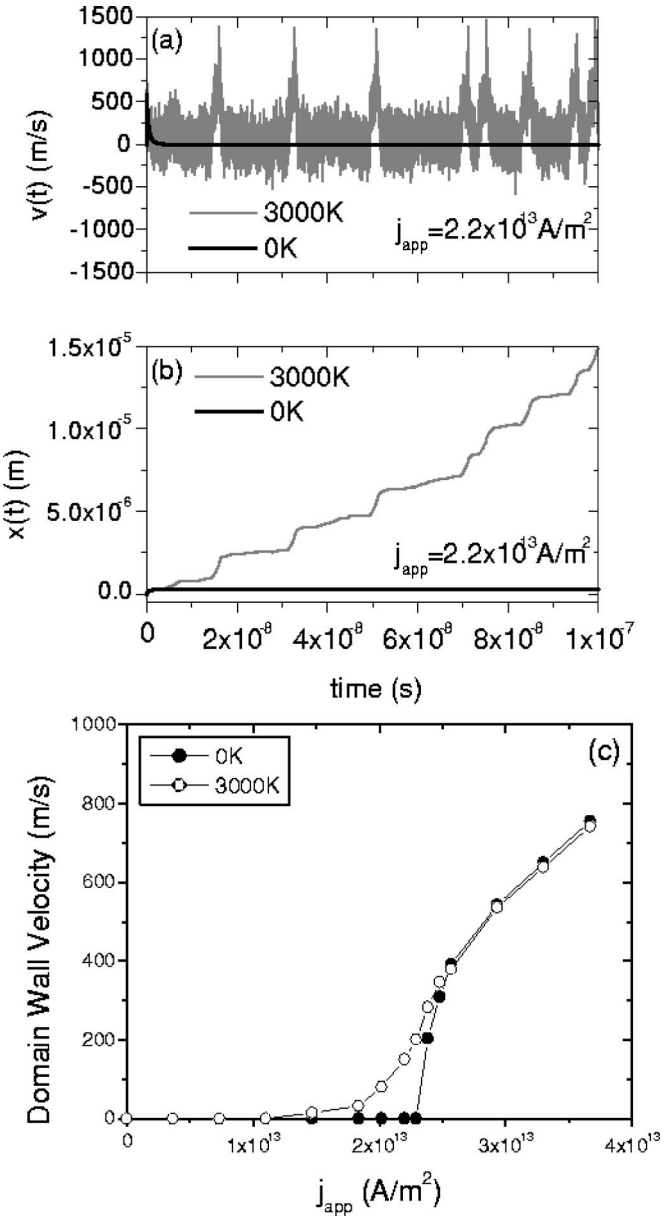

FIG. 5. Time evolution of DW (a) velocity and (b) displacement in the perfect adiabatic case ($\xi=0$) for $j_{app}=2.2\times10^{13}$ A/m^2 ($b_J=600$ m/s) and lateral dimensions 50×5 nm^2. Results at $T_{\mu M}=0$ K are compared with a typical stochastic trajectory at $T_{\mu M}=3000$ K. (c) DW velocity as function of the applied current.

contrast with the perfect adiabatic case, there is no threshold current, and DWM is observed for any value of the applied density current. On the other hand, the discrepancies between the deterministic ($T=0$ K) and thermally activated ($T_{\mu M}=3000$ K) cases are insignificant. Two regimes can be observed in Fig. 6(c). For $j_{app}<2.2\times10^{13}$ A/m^2, the structure and width of the DW during motion do not significantly change from the structure and width at rest, and the DW velocity depends linearly on the applied current. For larger currents ($j_{app}>2.2\times10^{13}$ A/m^2), the slope is reduced due to internal changes in the wall structure. In particular, it becomes asymmetric and an antivortex is nucleated at one edge. Our simulations reveal that the antivortex remains at

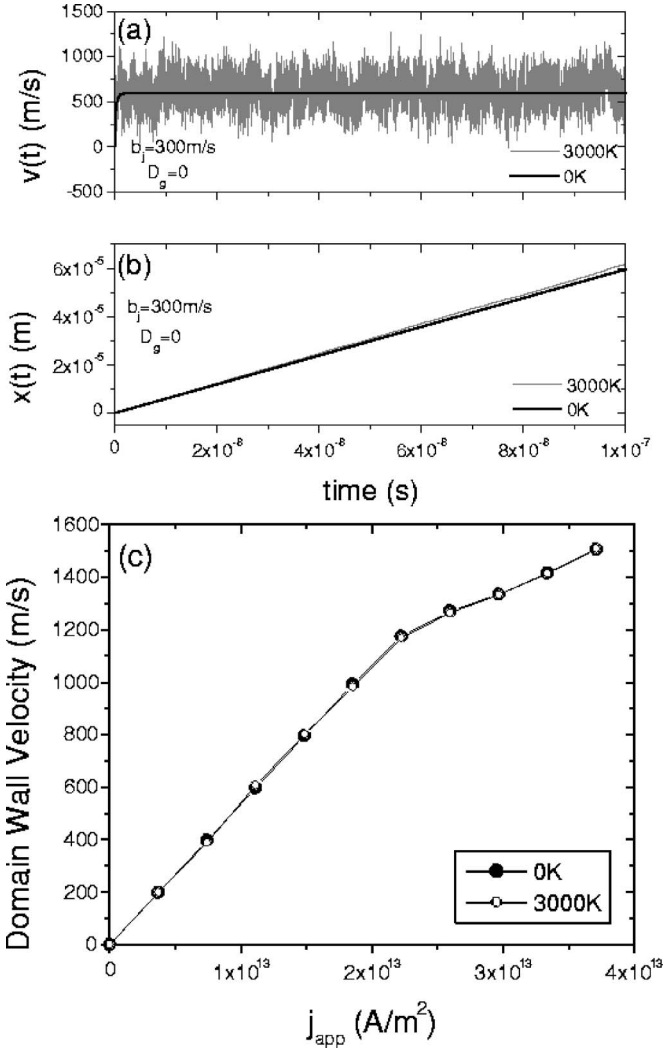

FIG. 6. Time evolution of DW (a) velocity $v(t)$ and (b) displacement $x(t)$ in the nonadiabatic case (ξ=0.04) at T=0 K and $T_{\mu M}$=3000 K for a perfect wire (D_g=0), $j_{app}=1.11\times10^{13}$ A/m^2 ($b_J\approx300$ m/s), and lateral dimensions 50×5 nm^2. (c) DW average velocity as function of the applied current.

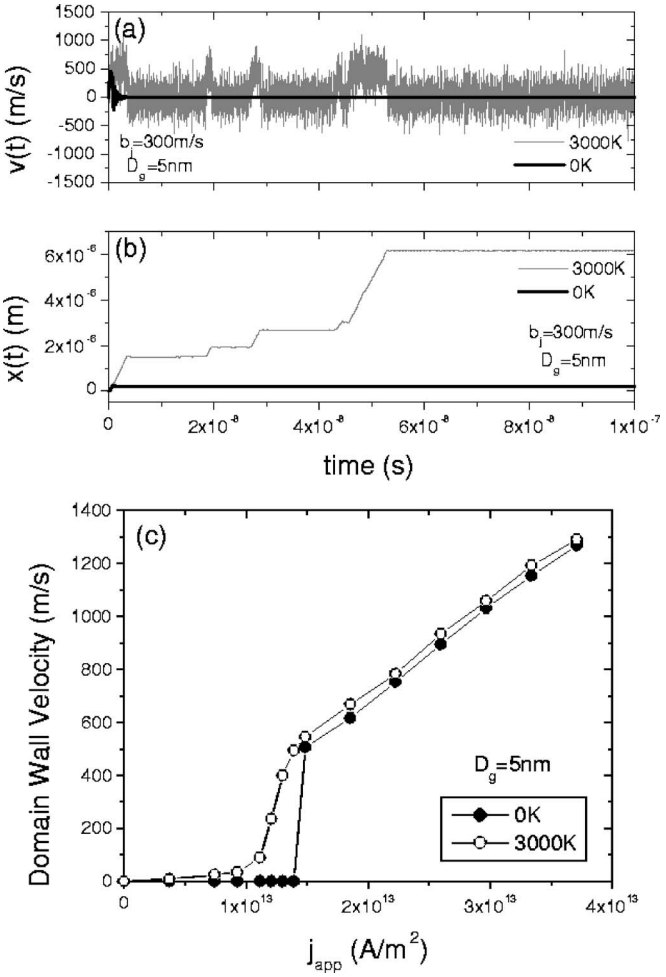

FIG. 7. Time evolution of DW (a) velocity and (b) displacement in the nonadiabatic case (ξ=0.04) at T=0 K and $T_{\mu M}$=3000 K for a wire of 50×5nm^2 cross section and roughness given by D_g=5 nm with an applied current density of $j_{app}=1.11\times10^{13}$A/m^2 ($b_J$=300 m/s). (c) DW averaged velocity as function of the applied current in the nonadiabatic case (ξ=0.04).

the edge during motion and does not propagate transversely in a temporal window of 100 ns.

2. *Rough wires* ($D_g\neq0$)

In Fig. 7, typical deterministic and stochastic trajectories of both DW (a) velocity and (b) position are depicted, whereas the average DW velocities as a function of the applied current are shown in Fig. 7(c). A typical roughness value of D_g=5 nm has been considered. As expected, roughness introduces coercivity in the system and, at $T_{\mu M}$=0 K, a minimum density current $j_{unp}(0\text{ K})=1.48\times10^{13}$ A/m^2 is required to unpin the DW. At this critical value, the DW velocity curve presents an abrupt rise from 0 to 507 m/s. For larger currents [$j_{app}>j_{unp}(0\text{ K})$], the DW velocity increases following an almost linear law as a function of j_{app}, but with a reduced slope with respect to the perfect case, due to the roughness. In this regime, the DW moves without significantly changing its internal structure and width. When thermal fluctuations are considered, a finite no-null average DW velocity is achieved for currents smaller than the deterministic unpinning threshold $j_{unp}(0\text{ K})$. An averaged velocity of $v\approx8.5$ m/s is reached at the effective micromagnetic temperature $T_{\mu M}$=3000 K when the applied current is $j_{app}=3.7\times10^{12}$ A/m^2, which is in good quantitative agreement with recent experimental measurements.[38] Moreover, as it was the case in field-driven DWM (Sec. III), in the thermally activated range [$j_{app}<j_{unp}(0\text{ K})$], the DW velocity increases exponentially with the current, which is also in good agreement with recent theoretical predictions[10,18] and experimental observations.[38,41] Therefore, our simulations suggest that the experimental DW velocity observations could be a consequence of the thermal activation over roughness energy barriers when the finite nonadiabatic corrections ($\xi>0$) are assumed. The validity of this statement must be tested by further experimental research along with more theoretical and numerical investigations. In the next section, we present a simple theoretical model with the aim of understanding the

basic principles behind our micromagnetic results from a more fundamental point of view.

V. ONE-DIMENSIONAL BROWNIAN MODEL

The model presented in this section treats the DW as a rigid object in a one-dimensional wire. This model (hereafter 1DM) was originally introduced to describe field-driven DWM (Refs. 1 and 2) and more recently extended to include spin-transfer torque effects.[9,13,16,27] Our contribution consists on adding thermal fluctuations and roughness to it as it will be discussed in Secs. V B and V C, respectively.

A. Deterministic one-dimensional model ($T=0$ K)

Starting from the Landau-Lifshitz equation and assuming a one-dimensional Bloch-like "tanh" profile for the domain wall, Schryer and Walker[1] derived simple analytical expressions for the DW width, velocity, and tilt angle as a function of the applied field. Moreover, assuming that the wall width and internal structure do not depend on the applied field and remain unchanged during motion, and also that the out-of-plane tilt angle is small, Li and Zhang[16] showed that it is possible to linearize the equations and arrive at the following Newton-like equation for DWM:

$$m_w \frac{dv_x}{dt} = F_{fri} + F_{ext,s}, \tag{9}$$

where m_w is the effective domain wall mass and F_{fri} and $F_{ext,s}$ are the friction and external forces, respectively. The domain wall mass is given by

$$m_w = 2(1+\alpha^2)\frac{\mu_0 L_y L_z}{\gamma_0^2 (N_z - N_y)\Delta_0}, \tag{10}$$

with N_y and N_z being the demagnetizing factors[52] corresponding to the wire cross-section dimensions and Δ_0 the domain wall width. The friction force F_{fri} is given by

$$F_{fri} = -\alpha(\mu_0 L_y L_z)\frac{2M_s}{\gamma_0 \Delta_0} v_x(t), \tag{11}$$

whereas the external force $F_{ext,s}$ has two contributions due to the external field ($F_{H,s}$) and the spin-polarized current ($F_{j,s}$), respectively,

$$F_{ext,s} = F_{H,s} + F_{j,s} = (\mu_0 L_y L_z)\left(2M_s H_{ext} - \frac{2M_s}{\gamma_0 \Delta_0} c_J\right). \tag{12}$$

Equation (9) allows us to describe the DW motion as a particle with an effective mass m_w subjected to both friction [Eq. (11)] and external forces [Eq. (12)] for perfect wires in the absence of thermal fluctuations.[53,54] The solution of Eq. (9) when time-independent external forces are instantaneously applied at $t=0$ is given by

$$v_x(t) = v_x(\infty)[1 - \exp(-t/t_R)] + v_x(0)\exp(-t/t_R), \tag{13}$$

where t_R is the relaxation time defined as

$$\frac{1}{t_R} = \frac{\alpha}{1+\alpha^2}\gamma_0 M_s (N_z - N_y) \tag{14}$$

and $v_x(0)$ and $v_x(\infty)$ are, respectively, the initial and terminal velocities given by

$$v_x(0) = -\frac{b_J}{1+\alpha^2}, \tag{15}$$

$$v_x(\infty) = \frac{1}{\alpha}[\gamma_0 \Delta(\infty) H_{ext} - c_J]. \tag{16}$$

Before introducing thermal fluctuations in the model, and in order to check its validity range, we compare its predictions with our micromagnetic simulations for a perfect wire ($D_g=0$) of 200×5 nm^2 cross section. Among the different possible definitions for the domain wall width, we have verified that the best fit with the simulations is obtained for Thiele's[3] definition $\Delta_{Th} = 2L_y M_s^2 / [\int (\partial \vec{M}/\partial x)^2 dxdy]$ which, in our case, yields a value of $\Delta_{Th}=43$ nm as computed from the micromagnetic configuration of the DW in static equilibrium.

The solution of the deterministic 1DM for field-driven DWM is presented in Fig. 8(a). When the wall width is assumed to be constant ($\Delta_0=43$ nm), the 1DM (black circles) predicts correct values for the terminal velocity $v_x(\infty)$ for small applied fields, but for $\mu_0 H_{ext} > 1$ mT, the discrepancies are significant and increase with the field. However, if the micromagnetic computed value for the terminal DW width $\Delta(\infty)$ is taken into account as an input parameter for solving the Newton equation [Eq. (9)] (black squares), the values predicted by the 1DM reproduce accurately the micromagnetic ones (white circles) for all field values below the breakdown Walker field ($\mu_0 H_W \approx 2.75$ mT). The steady-state DW width using Thiele's definition as a function of the external field is shown in the inset of Fig. 8(a). Above the breakdown field, the 1DM ceases to be valid because the internal changes of the wall structure cannot be qualitatively described within the one-dimensional approach.

The results for the current-driven case are shown in Fig. 8(b). The values computed from the 1DM are very close to the micromagnetic ones for applied currents smaller than $b_J \approx 600$ m/s ($\xi=0.04$) because in this range the micromagnetic terminal velocity does not depend on the domain wall width. For larger values, the micromagnetic results start to differ from the analytical ones because the internal structure of the wall becomes asymmetric. Fortunately, the experimental accessible range for the applied current is well below this region.

B. Stochastic one-dimensional model ($T\neq 0$ K)

To include thermal perturbations in the 1DM, we adopt Langevin's description of Brownian motion by adding a fluctuating random force $F_{th}(t)$ to the deterministic Eq. (9), consequently becoming an stochastic one as follows:

$$m_w \frac{dv_x}{dt} = F_{fri} + F_{ext,s} + F_{th}(t). \tag{17}$$

The thermal force $F_{th}(t)$ is a random Gaussian-distributed process with the following statistical properties:

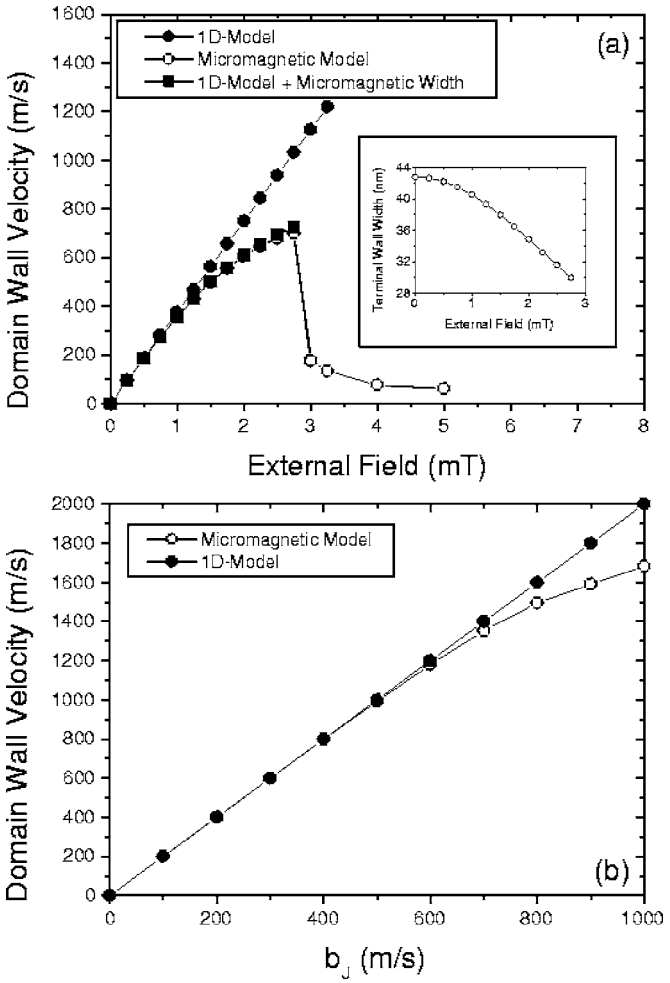

FIG. 8. DW velocity for a perfect wire of 200×5 nm^2 cross. The micromagnetic results are compared with the asymptotic solution ($t\gg t_R$) of the 1DM. (a) Field-driven DWM and (b) current-driven DWM (ξ=0.04).

$$\langle F_{th}(t)\rangle = 0, \tag{18}$$

$$\langle F_{th}(t)F_{th}(t')\rangle = 2D_{1D}\delta(t-t'). \tag{19}$$

The strength of the thermal force is given by D_{1D}, which needs to be obtained from the fluctuation-dissipation theorem.[47] If Eq. (17) is rewritten in terms of $\tilde{v}_x(t)=v_x(t)-v_x(\infty)$ as

$$\frac{d\tilde{v}_x(t)}{dt} = -\frac{\tilde{v}_x(t)}{t_R} + \frac{1}{m_w}F_{th}(t), \tag{20}$$

the Fokker-Planck equation corresponding to the Eq. (20), which determines the temporal evolution of the probability distribution $P(\tilde{v}_x(t),t)$ for the DW velocity, can be expressed as the following continuity equation:[47]

$$\frac{\partial P(\tilde{v}_x(t),t)}{\partial t} = -\frac{\partial J(\tilde{v}_x(t),t)}{\partial(\tilde{v}_x(t))}, \tag{21}$$

where the probability density current $J(\tilde{v}_x(t),t)$ is given by

$$J = \left[-\frac{\tilde{v}_x}{t_R} - \frac{D_{1D}}{m_w^2}\frac{\partial}{\partial\tilde{v}_x}\right]P. \tag{22}$$

By imposing Boltzmann's distribution, $P_B \propto \exp[-m_w\tilde{v}_x^2(t)/(2K_BT)]$, as a stationary solution of Eq. (21), the following expression for the D_{1D} is obtained:

$$D_{1D} = \frac{m_w}{t_R}K_BT. \tag{23}$$

With Eq. (23), the thermal field F_{th} during a time interval Δt can be written as

$$F_{th}(t) = \eta(t)\sqrt{2\frac{m_w}{t_R}\frac{K_BT}{\Delta t}}, \tag{24}$$

where $\eta(t)$ is a normalized zero-averaged Gaussian-distributed white-noise process. The solution of Eq. (20) with Eqs. (18) and (19) can be written as

$$\tilde{v}_x(t) = \tilde{v}_x(0)e^{-t/t_R} + e^{-t/t_R}\int_0^t \frac{F_{th}(t')}{m_w}e^{t'/t_R}dt'. \tag{25}$$

Averaging over many stochastic realizations ($\langle\cdots\rangle$), we obtain an expression for the velocity $\tilde{v}_x(t)$ as follows:

$$\langle\tilde{v}_x(t)\rangle = \tilde{v}_x(0)e^{-t/t_R}, \tag{26}$$

which is analogous to the deterministic solution [Eq. (13)]. This is consistent with the results from micromagnetic simulations for wires with no surface roughness presented in the previous sections [see Figs. 2(c) and 6(c)]. Consequently, we can conclude that thermal perturbations have no net effect on DWM in perfect wires.

C. Including the roughness

In the field-driven DWM case, edge roughness of characteristic size D_g is introduced in the model by means of a local pinning force $F_{pin}(x)=-(\mu_0L_yL_z)2M_sH_{pin}(x)$, where the local pinning field $H_{pin}(x)$ is randomly generated with a uniform distribution of maximum value given by the unpinning field $H_{unp}(0\text{ K})$ corresponding to the typical roughness size D_g as calculated micromagnetically [Fig. 3(a)]. The roughness is assumed to be uniform over a distance given by the DW width computed micromagnetically for the wire dimensions considered.

Typical trajectories of the DW velocity and position as predicted by our model are shown in Fig. 9. The applied field is μ_0H_{ext}=2.5 mT and the wire dimensions are the same as in Sec. III. The maximum pinning field is $\mu_0H_{pin}(x)$=4 mT, which corresponds to a surface roughness given by D_g =25 nm. The 1DM trajectories depict similar features than micromagnetic simulations (see Fig. 4). At T=0 K, the DW moves until it becomes pinned at a position where the local pinning field is higher than the external field. On the contrary, at room temperature (T=300 K), due to thermal perturbations, the wall remains pinned at different places only for a finite time interval.

In Fig. 10, the DW averaged velocity (over 100 stochastic realizations in a temporal window of 100 ns) as a function of

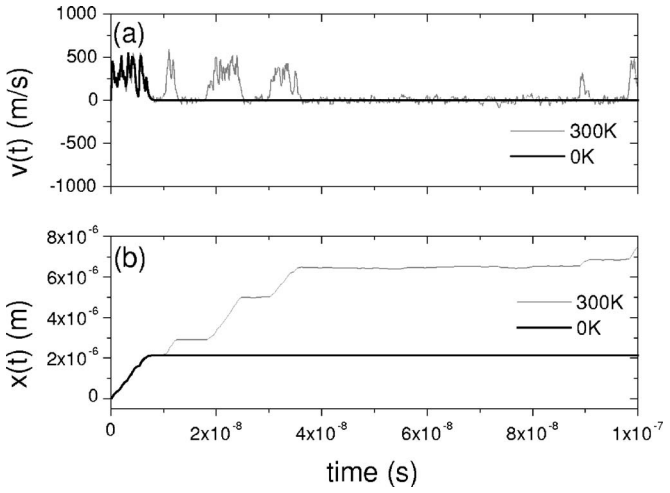

FIG. 9. DW (a) velocity $v(t)$ and (b) displacement $x(t)$ trajectories predicted by the 1DM for a wire with roughness given by D_g =25 nm and lateral dimensions 200×5 nm^2. The applied field is $\mu_0 H_{ext}$=2.5 mT and the maximum local pinning field is $\mu_0 H_{unp}$(0 K)=4 mT. Both deterministic (T=0 K) and room-temperature (T=300 K) trajectories are shown.

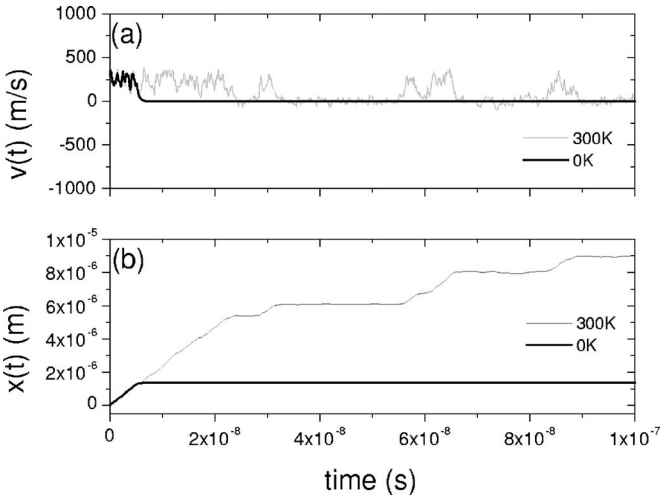

FIG. 11. Time evolution of DW (a) velocity $v(t)$ and (b) position $x(t)$ as predicted by the 1DM for a wire of lateral dimensions 50 $\times5$ nm^2 and roughness given by D_g=5 nm. The applied current is $j_{app}=1.11\times10^{13}$ A/m^2 and the maximum pinning current is $j_{unp}(0\text{ K})=1.5\times10^{13}$ A/m^2. Both deterministic (T=0 K) and room-temperature (T=300 K) trajectories are shown.

the applied field predicted by the 1DM is compared with both micromagnetic simulations and experimental measurements.[33] As can be observed, a remarkable good agreement among the three curves is obtained in the thermally activated range (2 mT$<\mu_0 H_{ext}<$3.5 mT). It is worth pointing out that there is no fitting parameter in the 1DM and that the results have been obtained using T=300 K, whereas, as it was discussed in Sec. III, an effective micromagnetic temperature value of $T_{\mu M}$=3000 K was used in the micromagnetic simulations. For larger fields, $H_{ext}>H_{unp}$(0 K), the increasing discrepancy between the 1DM and the simulations is due to the fact that, as discussed in Sec. V A, the former assumes that the DW width is independent of the applied field and does not take into account the changes in the DW structure that take place in this region.

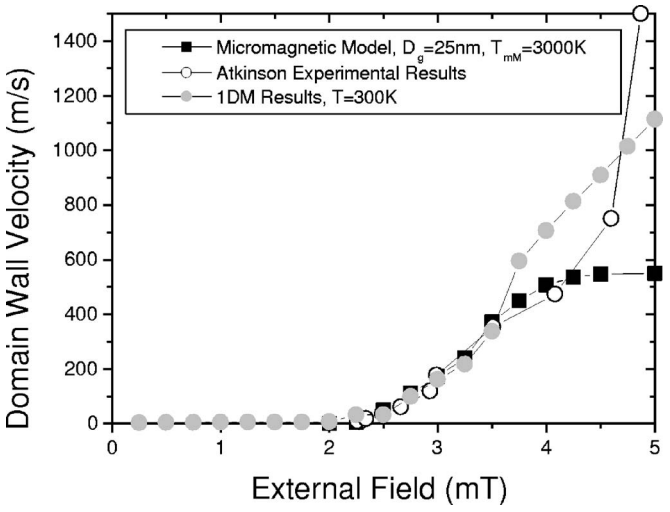

FIG. 10. Average domain wall velocity as a function of the applied field for a permalloy wire of 200×5 nm^2 rectangular section. One-dimensional results at room temperature are compared with both micromagnetic and experimental ones of Fig. 3(c).

Following a similar procedure than the one described above, in the current-driven DWM case, edge roughness of characteristic size D_g is introduced in the model by means of a local pinning force $F_{pin}(x)=(\mu_0 L_y L_z)(2M_s/\gamma_0\Delta_0)c_{J,pin}(x)$, where $c_{J,pin}=j_{pin}(x)[\xi\mu_B P/(eM_s)]$. $j_{pin}(x)$ is a spatially dependent pinning current randomly generated with a uniform distribution of maximum value given by the unpinning current j_{ump}(0 K) corresponding to the typical roughness size D_g as calculated by means of micromagnetic simulations in Sec. IV. Again, the roughness is assumed to be uniform over a distance given by the DW width computed micromagnetically for the wire dimensions considered. In the results that follow, nonadiabatic corrections with ξ=0.04 and the same wire dimensions than in Sec. IV (50×5 nm^2) are assumed. Based on micromagnetic results at T=0 K [see Fig. 7(c)], a local pinning current distribution with a maximum value of $j_{unp}(0\text{ K})=1.5\times10^{13}$ A/m^2, corresponding to a surface roughness given by D_g=5 nm, has been considered.

Figure 11 shows typical deterministic and room-temperature trajectories as predicted by the 1DM for j_{app} $=1.11\times10^{13}$ A/m$^2<j_{unp}$(0 K). As can be observed, the same features of micromagnetic simulations [see Figs. 7(a) and 7(b)] are captured by our extended 1DM. From a quantitative point of view, the average DW velocity over 100 stochastic realizations for a temporal window of 100 ns computed by means of the 1DM at T=300 K is compared in Fig. 12 with the micromagnetic results of Fig. 7(c). For currents larger than the deterministic threshold [$j_{app}>j_{unp}$(0 K)], the DW velocity increases linearly with j_{app}, but, as in the field-driven case, the slope in this linear range is larger for the 1DM than for the micromagnetic simulations because, as mentioned before, the former does not take into account in-

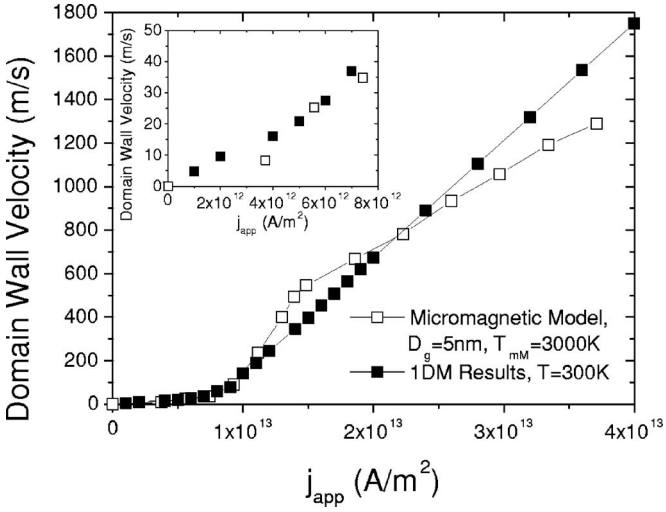

FIG. 12. Average domain wall velocity as a function of the applied current for a permalloy wire of 50×5 nm^2 rectangular cross section. Results predicted by the 1DM at room temperature are compared with micromagnetic ones of Fig. 7(c).

ternal structural changes inside the DW that take place when the driving force, either field or current, is large. On the other hand, in the thermally activated regime $[j_{app}<j_{unp}(0\ \mathrm{K})]$, the DW velocity follows an exponential increase with j_{app} and a better agreement between both models is obtained. Finally, the inset of Fig. 12 shows the computed averaged velocities in the experimentally accessible range of applied currents. A DW velocity of $v\approx6$ m/s is deduced for an applied density current of $j_{app}=10^{12}$ A/m^2. This value is in good agreement with the experimental measurements in Refs. 38 and confirms the key role of thermal effects.

VI. CONCLUSIONS

A systematic analysis of the motion of transverse domain walls driven by either an external field or an in-plane current in wires of rectangular cross section has been carried out by means of micromagnetic simulations with emphasis on investigating the role of thermal perturbations. A one-dimensional model has also been used to complement the investigation. This model, originally derived by Li *et al.*, has been extended to include thermal perturbations and roughness.

In general, it is found that, when the driving force, either field or current, is larger than the pinning force, thermal perturbations have a negligible effect on the DW velocity, which is found to depend linearly on the external force. On the contrary, when the external force is below the deterministic propagation threshold, thermal activation over pinning energy barriers leads to no-null velocities. In this thermally activated regime, the DW velocity is found to depend exponentially on the external force. Moreover, our results show that the inclusion of thermal perturbations and roughness is crucial in order to reduce the discrepancies between experimental measurements and theoretical predictions.

In particular, in the field-driven case, both micromagnetic simulations and 1DM show a good quantitative agreement with the experimental data obtained by Atkinson *et al.*[33] for a wide field range using a value of $D_g=25$ nm for the size that characterizes the roughness. Similarly, in the current-driven case, the computed velocities are of the same order of magnitude than those reported in Refs. 38 choosing a value $D_g=5$ nm if the nonadiabatic approximation with $\xi=0.04$ is considered.

ACKNOWLEDGMENTS

We thank D. Atkinson *et al.* for providing the experimental values of Ref. 33 and valuable comments. This work was partially supported by Projects No. MAT2005-04827 from the Spanish Government and No. SA063A05 from Junta de Castilla y Leon.

*Electronic address: emvecino@ubu.es

[1] N. L. Schryer and L. R. Walker, J. Appl. Phys. **45**, 5406 (1974).
[2] J. C. Slonczewski, Int. J. Magn. **2**, 85 (1972); A. P. Malozemoff and J. C. Slonczewski, *Magnetic Domains Walls in Bubble Materials* (Academic, New York, 1979).
[3] A. A. Thiele, Phys. Rev. Lett. **30**, 230 (1973).
[4] L. Berger, J. Appl. Phys. **55**, 1954 (1984); Phys. Rev. B **33**, 1572 (1986).
[5] J. C. Slonczewski, J. Magn. Magn. Mater. **159**, L1 (1996).
[6] Y. B. Bazaliy, B. A. Jones, and Shou-Cheng Zhang, Phys. Rev. B **57**, R3213 (1998).
[7] S. Zhang, P. M. Levy, and A. Fert, Phys. Rev. Lett. **88**, 236601 (2002).
[8] X. Waintal and M. Viret, Europhys. Lett. **65**, 427 (2004).
[9] G. Tatara and K. Kohno, Phys. Rev. Lett. **92**, 086601 (2004).
[10] S. E. Barnes and S. Maekawa, Phys. Rev. Lett. **95**, 107204 (2005).
[11] J. Shiabata, G. Tatara, H. Hohno, and Y. Otani, IEEE Trans. Magn. **41**, 2595 (2005).
[12] V. K. Dugaed, V. R. Vieira, P. D. Sacramento, J. Barnas, M. A. N. Araujo, and J. Berakdar, arXiv:cond-mat/0509574 (unpublished).
[13] S. Zhang and Z. Li, Phys. Rev. Lett. **93**, 127204 (2004).
[14] Z. Li and S. Zhang, Phys. Rev. B **70**, 024417 (2004).
[15] Z. Li, J. He, and S. Zhang, J. Appl. Phys. **97**, 10C703 (2005).
[16] Z. Li, J. He, and S. Zhang, J. Appl. Phys. **99**, 08Q702 (2006).
[17] Peng-Bin He, X. C. Xie, and W. M. Liu, Phys. Rev. B **72**, 172411 (2005).
[18] G. Tatara, N. Vernier, and J. Ferre, Appl. Phys. Lett. **86**, 252509 (2005).
[19] X. Liu, X. J. Liu, and Z. X. Lui, arXiv:cond-mat/0511069 (unpublished).
[20] J. I. Ohe and B. Kramer, Phys. Rev. Lett. **96**, 027204 (2006).
[21] R. D. McMichael and M. J. Donahue, IEEE Trans. Magn. **33**, 4167 (1997).
[22] D. G. Porter and M. J. Donahue, J. Appl. Phys. **95**, 6729 (2004).

[23] Y. Nakatani, A. Thiaville, and J. Miltat, Nat. Mater. **2**, 521 (2003).
[24] Y. Nakatani, A. Thiaville, and J. Miltat, J. Magn. Magn. Mater. **290**, 750 (2005).
[25] A. Thiaville, J. M. Garcia, and J. Miltat, J. Magn. Magn. Mater. **242-245**, 1061 (2002).
[26] A. Thiaville, Y. Nakatani, J. Miltat, and N. Vernier, J. Appl. Phys. **95**, 7049 (2004).
[27] A. Thiaville, Y. Nakatani, J. Miltat, and Y. Suzuki, Europhys. Lett. **69**, 990 (2005).
[28] J. He, Z. Li, and S. Zhang, J. Appl. Phys. **98**, 016108 (2005).
[29] S. S. P. Parkin, U.S. Patent No. 6,834,005 (21 December 2004).
[30] D. A. Allwood, G. Xiong, C. C. Faulkner, D. Atkinson, D. Petit, and R. P. Cowburn, Science **309**, 1688 (2005).
[31] T. Ono, H. Miyajima, K. Shigeto, K. Mibu, N. Hosoito, and T. Shinjo, Science **284**, 468 (1999).
[32] G. S. D. Beach, C. Nistor, C. Knutson, M. Tsoi, and J. L. Erskine, Nat. Mater. **4**, 741 (2005).
[33] D. Atkinson, D. A. Allwood, G. Xiong, M. D. Cooke, and R. P. Cowburn, Nat. Mater. **2**, 85 (2003).
[34] A. Kirilyuk, J. Ferre, V. Grolier, J. P. Jamet, and D. Renard, J. Magn. Magn. Mater. **171**, 45 (1997).
[35] F. Cayssol, D. Ravelosona, J. Wunderlich, C. Chapert, V. Mathet, J. P. Jamel, and J. Ferre, J. Magn. Magn. Mater. **240**, 30 (2002).
[36] M. Klaui, H. Ehrke, U. Rudiger, T. Kasama, R. E. Dunin-Borkowski, D. Backes, L. J. Heyderman, C. A. F. Vaz, J. A. C. Bland, G. Faini, E. Cambril, and W. Wernsdorfer, Appl. Phys. Lett. **87**, 102509 (2005).
[37] M. Laufenberg, D. Backes, W. Buhrer, M. Klaui, U. Rudiger, C. A. F. Vaz, J. A. C. Bland, L. J. Heyderman, F. Nolting, S. Cherifi, A. Locatelli, R. Belkhon, S. Heun, and E. Bauer, Appl. Phys. Lett. **88**, 052507 (2006).
[38] A. Yamaguchi, T. Ono, S. Nasu, K. Miyake, K. Mibu, and T. Shinjo, Phys. Rev. Lett. **92**, 077205 (2004).
[39] A. Yamaguchi, S. Nasu, H. Tanigawa, T. Ono, K. Miyake, K. Mibu, and T. Shinjo, Appl. Phys. Lett. **86**, 012511 (2005).
[40] N. Vernier, D. A. Allwood, D. Atkinson, M. D. Cooke, and R. P. Cowburn, Europhys. Lett. **65**, 526 (2004).
[41] D. Ravelosona, D. Lacour, J. A. Katine, B. D. Terris, and C. Chappert, Phys. Rev. Lett. **95**, 117203 (2005).
[42] W. F. Brown, Phys. Rev. **130**, 1677 (1963).
[43] J. L. Garcia-Palacios and F. J. Lazaro, Phys. Rev. B **58**, 14937 (1998).
[44] M. J. Donahue and R. D. McMichael, Physica B **233**, 272 (1997); M. J. Donahue, J. Appl. Phys. **83**, 6491 (1998).
[45] A. J. Newell, W. Willians, and D. J. Dunlop, J. Geophys. Res. **98**, 9551 (1993).
[46] S. Chykazumi, *Physics of Magnetism* (Wiley, New York, 1964), p. 272.
[47] P. E. Kloeden and E. Platen, *Numerical Solution of Stochastic Differential Equations*, Applications of Mathematics, Vol. 23 (Springer-Verlag, Berlin, 1995).
[48] Considering the values of the intrinsic parameters (Sec. II) and the cell size used in the simulations (Δx=5 nm), the ferromagnetic order breakdown occurs at around $T=10^4$ K, which is about 1 order of magnitude higher than the Curie temperature of permalloy.
[49] G. Grinstein and R. H. Koch, Phys. Rev. Lett. **90**, 207201 (2003).
[50] The measurements at position I, however, are taken after the wall has traveled through an L turn and, therefore, are not directly compared with our results.
[51] G. Bertotti, *Hysteresis in Magnetism* (Academic, San Diego, 1998).
[52] A. Aharoni, J. Appl. Phys. **83**, 3432 (1998).
[53] Analogous derivation of the deterministic Eq. (9) can be seen in Refs. 16 and 17. In the mentioned papers, thin-film approximation ($L_z \to \infty$) was assumed. Our derivation of Eq. (9) includes the thickness-to-width ratio (L_z/L_y) dependence of the demagnetizing field via Ref. 52, and, consequently, an explicit dependence of DW mass on thickness-to-width section of the wire can be inferred. The thin-film approximation is straightforwardly recovered by assuming $N_z=1$ and $N_y=0$.
[54] The one-dimensional model can be completed by including the effect of time-dependent external forces ($F_{ext,d}$) on the right-hand side of Eq. (9), $F_{ext,d}=F_{H,d}+F_{j,d}=\frac{2(\mu_0 L_y L_z)}{\gamma_0(N_z-N_y)}\left[\alpha\frac{\partial H_{ext}}{\partial t}-\frac{(1+\alpha\xi)}{\gamma_0\Delta_0}\frac{\partial b_J}{\partial t}\right]$. The consequences of these time-dependent forces will be analyzed elsewhere.